Characterization of shallow marine sediments using high-resolution velocity analysis and genetic algorithms driven 1D elastic full-waveform inversion

Aleardi M., Tognarelli A., Mazzotti A.

University Of Pisa, Earth Sciences Department, via S. Maria 53, 56126, Pisa

Abstract

We estimate the elastic properties of marine sediments beneath the seabed by means of high-resolution velocity analysis and 1D elastic full-waveform inversion (FWI) performed on 2D broad-band seismic data of a well-site survey. A high-resolution velocity functional is employed to exploit the broad frequency band of the data and to derive the P-wave velocity field with a high degree of accuracy. To derive a complete elastic characterization in terms of P-wave, S-wave velocities (*Vp, Vs*) and density of the subsurface, and to increase the resolution of the *Vp* estimates, we apply a 1D elastic full-waveform inversion in which the outcomes derived from the velocity analysis are used as a priori information to define the *Vp* search range. The 1D inversion is solved by making use of genetic algorithms (GAs) as the optimization method and it is performed by considering two misfit functions: the first uses the entire waveform to compute the misfit between modelled and observed seismograms; the second considers the envelope of the seismograms, thus relaxing the requirement of an exact estimation of the wavelet phase. The full-waveform inversion and the high-resolution velocity analysis yield comparable *Vp* profiles but the FWI reconstruction is much more detailed. For what concerns the full-waveform inversion results, the final depth models of P-wave and S-wave velocities and density show a fine layered structure with a significant increase of velocities and density at shallow depth, which may indicate the occurrence of a consolidated layer. The very similar velocities and density depth trends obtained by employing the two different misfit functions increase our confidence in the reliability of the predicted subsurface model.

1. Introduction

The increase in offshore exploration, and related construction activity, requires a reliable characterization of the seabed and of the shallow subsurface in order to minimize the risk of harming personnel and equipment during drilling operations, to prevent accidents to the natural environment and to identify safe zones for the installation of underwater structures such as platforms and pipelines. To this end, seismic data are often used to predict the properties of seafloor sediments and to identify possible shallow hazards (Mallick and Dutta, 2002; Riedel and Theilen, 2001; Riedel *et al*, 2003; Aleardi, 2015a; Aleardi and Tognarelli 2016). Changes in depth or in space of the velocity field are the leading indicators to detect variations in physical properties of the seafloor sediments.

Velocity analysis is the processing step used to build a velocity model and the semblance functional (Neidell and Taner, 1971) is commonly used to compute velocity spectra. Semblance is fast to compute and robust against uncorrelated noise, but it yields low-resolution spectra able to delineate only a general trend of the velocities. If a higher resolution is required other methods are needed. In this work, we employ the hybrid functional introduced by Tognarelli *et al.* (2013) that is obtained by weighting the Key and Smithson's (1990) signal-to-noise (S/N) ratio estimate by the complex matched functional (Spagnolini *et al.* 1993). The use of this hybrid functional allows us to take advantage of the combined use of a complex matched filter based on a priori knowledge of the source wavelet and of the coherency measure obtained by the eigenstructure analysis of the data covariance matrix. This makes it possible to evaluate high-resolution (HR) velocity spectra able to minimize the uncertainty in the picking of the time-velocity pairs and thus to derive a compressional velocity (*Vp*) field which, in case of nearly horizontal layers (as it is the case in the studied area), is quite accurate. The derived compressional velocity field can be useful for a preliminary interpretation or for deriving a priori constraints for further investigations, such as to constrain the search ranges of a stochastic full-waveform inversion (FWI) as done in the present work.

Full-waveform inversion is a data-fitting procedure based on full-wavefield modeling, which exploits the full information content of the recorded seismic data to derive high-resolution quantitative models of the subsurface (Virieux and Operto, 2009). Over the last decade most FWI developments have focused on building a compressional velocity field from low frequencies to be used as an improved background model for wave equation depth migration (Sirgue *et al.* 2010; Prieux *et al.* 2011; Morgan *et al.* 2013). In this context, 2D or 3D full-waveform inversion is usually solved in the acoustic approximation and applying gradient-based methods (such as steepest descent or conjugate gradient). On the one hand, gradient-based methods make it possible to invert for a large number of unknown model parameters. On the other hand, the limitation of describing the subsurface as an acoustic model is needed to reduce the computational cost, the non-linearity and the ill-posedness of the inverse problem. For example, it is well known (Operto et al., 2013) that the non-linearity in full-waveform inversion increases when many wave phenomena (multiples or converted waves) or different model parameters (*Vp, Vs*, density, viscoelastic and anisotropic parameters) are simultaneously considered in the inversion. It is clear that a prerequisite for the success of gradient-based FWI is the availability of a good starting model to prevent the inversion to be stuck in local minima and, to this end, several methods have been developed (Vireux and Operto, 2009; Sajeva *et al.* 2014a; Diouane *et al.* 2014; Tognarelli *et al.* 2015; Sajeva *et al.* 2016a).

Stochastic global search algorithms, such as simulated annealing, neighborhood or genetic algorithms (GAs) are other methods that are often applied to tackle the high non-linearity inherent to elastic FWI and to avoid the need of a good starting model not only for *Vp* but also for *Vs* and density parameters (Mallick, 1999; Fliedner *et al.* 2012; Li and Mallick, 2015; Aleardi and Mazzotti 2014). The advantage of using global search methods over the gradient-based ones is that they explore a wide region of the entire model space and that they can jump out from local minima. However, global optimization algorithms become computationally unfeasible when a large number of unknowns is considered. In the global approach to elastic FWI this drawback is usually avoided by assuming a 1D subsurface model, thus greatly reducing the number of inverted model parameters.

In this work, the simple layered nature of the investigated area characterized by moderate lateral changes in the elastic properties allow us to assume local 1D models in the neighborhood of few adjacent common-mid-point (CDP) gathers. Moreover, focusing the attention on the shallowest part of the subsurface further reduces the number of inverted model parameters. In addition, in our approach to 1D elastic full-waveform inversion the computational effort is further reduced by exploiting the accuracy of the velocity field derived from the high-resolution velocity analysis, which allows us to narrow the search range of the model space explored during the stochastic optimization. Among the many global optimization methods, we make use of a genetic algorithm as it results a very efficient method in solving the 1D elastic FWI (Sajeva *et al.* 2014b). In addition, in the stochastic full-waveform inversion a large number of unrelated and independent forward problems are separately solved with little or no communication among different tasks. This makes it possible for a parallel implementation that greatly reduces the computational cost of the inversion. In particular, we use a parallel algorithm implemented through a message passing interface communication protocol to speed up the inversion process.

We start describing the processing of the well-site survey seismic data aimed at deriving the final stack image, and at preparing the data for the high-resolution velocity analysis from which we derive the preliminary P-wave velocity field and information about the geological setting of the subsurface. The *Vp*, *Vs* and density characterization of the subsurface is then obtained by means of 1D elastic FWI. To this end, we follow two different approaches: in the first the entire waveform is considered in the inversion, whereas in the second only the envelopes of the seismic traces are taken into account, making it possible to relax the assumption of a perfect estimation of the phase of the source signature. These two approaches to full-waveform inversion allow us to analyze the possible benefits and/or drawbacks of introducing the envelope in the inversion.

2. Field data processing

The data considered in this work pertain to a 2D well-site survey seismic line acquired off-shore. A very simple geological setting and a shallow and nearly flat seafloor characterize the investigated area. Table 1 reports the most important recording and acquisition parameters: the short source and receiver spacings, the broad-band energy source, the limited maximum offset and the short sample interval clearly evidence the goal of the survey that is the high-resolution exploration of the seafloor and shallow layers.

Figure 1 illustrates a raw shot gather and the corresponding average spectrum, which exhibits a bandwidth between 10 Hz and more than 150 Hz. Low frequency noise can be recognized both in time and in the frequency spectrum close to 5 Hz. The flow chart of the processing sequence is shown in Figure 2. We adopt a conventional processing for marine data, paying particular attention at preserving and/or recovering the true amplitude of the signal (Mazzotti and Ravagnan, 1995; tognarelli xxxxxx) and without employing multichannel operator such as f-x deconvolution, tau-p filter or any kind of amplitude boost. The data obtained after predictive deconvolution are used to perform the high-resolution velocity analysis. The red arrows indicate that the input data for the 1D full-waveform inversion are the band-pass filtered raw gathers and the velocity field resulting from the high-resolution velocity analysis

The final time migrated section is illustrated in Figure 3. Being the nominal bin spacing equal to 6.25 m, the length of the profile is equal to 3 km, approximately. The section shows a simple geological setting with a flat sea bottom and horizontal layers down to 500 ms that gently dip below 600 ms. The limited depth penetration of the high frequency content of the signal is particularly evident by comparing the reflections above 500 ms and below 500 ms. For this reason only the shallowest part of the subsurface (down to 500 ms) is considered in the high-resolution velocity analysis and in the FWI tests.

3. High-resolution velocity analysis for deriving a compressional wave velocity field

The processing step known as velocity analysis is aimed at estimating a velocity model of the subsurface. It consists in the interpretation of velocity spectra and, in particular, in the picking of optimal time-velocity pairs (T_0-V) at different locations along the profile. The velocity spectra are computed estimating the signal coherence along hyperbolic traveltime trajectories. Coherency estimators yield quantitative information regarding the degree of similarity between signals among data traces. They can be derived taking into account the energy of the trace samples selected along trial traveltime hyperbolic trajectories, or they can evaluate the signal-to-noise ratio along the same trajectories, or else they can be computed by cross-correlating the traces in the specific time windows. Many estimators are available with different implementations and acting in different domains (Neidell and Taner, 1971; Jones and Levy 1987; Sguazzero and Vesnaver 1987; Biondi and Kostov 1989; Key and Smithson 1990; Spagnolini *et al.* 1993; Sacchi 1998; Grandi *et al.* 2007; Larner and Celis 2007; Abbad *et al.* 2009; Abbad and Ursin 2012; Tognarelli *et al.* 2013). Each of them differs in terms of resolution and capability to discriminate between signal and random and non-random noise (Ashton et al. 1994; Jones, 2010). In this work, we employ a high-resolution coherency estimator in the attempt to exploit the high-frequency content of the records and to overcome the low detectability of the reflection velocities due to the limited offset of the streamer.

The semblance functional C_{sem} (Neidell and Taner, 1971) is the most commonly used estimator and is defined as the ratio between the energy computed on a time window centered along a trial hyperbolic trajectory and the total energy on the same window:

$$C_{sem} = \frac{1}{M} \frac{\sum_{t=t_0-T/2}^{t=t_0+T/2} \left(\sum_{i=1}^{M} d_i(t_0; v_{stack}) \right)^2}{\sum_{t=t_0-T/2}^{t=t_0+T/2} \sum_{i=1}^{M} d_i^2 (t_0; v_{stack})}, \tag{1}$$

where i is the index of the M traces of the gather d and T is the width of the time window. The semblance measure typically produces a low-resolution velocity spectrum if events are close in time, if the move outs are small compared with the dominant period of the wavelet and if primaries interfere with other events such as converted waves and/or residual multiples. The semblance functional is useful to derive a velocity field for normal move-out (NMO) correction but is not appropriate to define a velocity field for a more accurate characterization of the subsurface.

A more sophisticated and higher resolution coherency estimator can be developed combining a quantitative estimate of the S/N ratio with a modification of the semblance functional in which we make use of the complex trace filtered by a source wavelet. Key and Smithson (1990), making use of the eigen-decomposition of the data covariance matrix, provide a mean to estimate the S/N ratio as follow:

$$S/N = \frac{\lambda_1 - \sum_{i=2}^{M} \frac{\lambda_i}{(M-1)}}{\sum_{i=2}^{M} \frac{\lambda_i}{(M-1)}} \qquad (2)$$

in which M is the number of traces and λ_i are the eigenvalues of the data covariance matrix.

An improved semblance functional can be derived transforming the input data traces into the complex domain by applying the Hilbert transform, and then filtering the data with a known source wavelet. Spagnolini *et al.* (1993) showed the improvement in the accuracy of the coherency measure even if making use of an approximate source wavelet to filter the data. They call this estimator *complex matched semblance* (C_{cms}):

$$C_{cms} = \frac{1}{M} \frac{\sum_{t=t_0-T/2}^{t=t_0+T/2} \left| \sum_{i=1}^{M} (D_i; t_0, v_{stack}) \right|^2}{\sum_{t=t_0-T/2}^{t=t_0+T/2} \sum_{i=1}^{M} \left| (D_i; t_0, v_{stack}) \right|^2}, \qquad (3)$$

where D represents the seismic data filtered by the source wavelet. As described in Tognarelli *et al.* (2013), we finally weight the complex matched semblance coefficient (equation 3) with the Key and Smithson's S/N ratio estimate of equation 2 to obtain

$$C_{cmsKS} = S/N \cdot C_{cms}, \qquad (4)$$

In Figure 4 the velocity spectra computed with the standard semblance estimator (C_{sem}) of equation 1 and the spectra computed with the hybrid measure C_{cmsKS} of equation 4 are compared for four CDP gathers. All the velocity spectra are represented from the arrival time of the seabed reflection (0.1 s, approximately) down to 0.52 s. The semblance velocity panels shown in Figure 4a exhibit broad peaks of high coherency and thus, a strong uncertainty in the definition of the time-velocity pairs arises. Instead, employing the hybrid estimator produces high-resolution velocity panels (Figure 4b) that make it possible to pick with a high degree of confidence the velocity trend of the primary reflections. An example of picking is shown in Figure 4c and Figure 4d. In particular, Figure 4d illustrates the picking (white dots) performed on the C_{cmsKS} panel for CDP 65. The same picked time-velocity pairs superimposed on the C_{sem} velocity map (Figure 4c) highlight the greater ambiguities in the picking if this had been performed on the semblance velocity spectrum.

We exploit the higher resolution and accuracy of the C_{cmsKS} panels to pick the velocity trend of the primaries and, taking advantage of the layer cake structure, we reconstruct a root mean square (V_{rms}) velocity model at each CDP location. The local 1D assumption is confirmed by the picked time-velocity pairs that remain quite constant for several adjacent CDP gathers and that slowly vary along the seismic line. This allows us to convert the V_{rms} model into interval velocity in depth using the simple Dix equation. The resulting P-wave velocity model is shown in Figure 5 superimposed to the depth migrated section. As expected, the derived velocity model reflects the simple geology with flat and nearly horizontal layers. The main Vp contrasts are related to the seabed and to two reflectors located at 280 m and 360 m, approximately.

4. 1D elastic full-waveform inversion

As previously introduced, to solve the 1D elastic full-waveform inversion we use the genetic algorithm method. Genetic algorithms (Holland 1975, Goldberg 1989, Mitchell 1998, Sivanandam and Deepa 2008) are a class of search methods that belong to the larger class of evolutionary algorithms. They use the principles of natural selection and evolution to search through model space for optimal solutions. The optimization starts with randomly generated individuals, each one encoding a candidate solution, and the entire population of individuals is evolved toward better solutions by using three principal evolutionary principles: selection, cross-over and mutation. At each generation (i.e. iteration) the fitness that is the goodness, of each individual is evaluated and then some individuals (parents) are stochastically selected from the current population on the basis of their fitness value. Next, they are modified (using cross-over and mutation) to form a set of offspring that are used to replace the least fitting parents and to form the new population that is used in the next generation. The algorithm usually terminates when either a maximum number of generations has been produced, or a satisfactory fitness level has been reached. Being aware of the inherent stochastic nature of the genetic algorithm full-waveform inversion, that is the inversion results can differ for different inversion runs, we performed 6 different inversions for each considered CDP gather and the final result is the predicted model that produces the minimum L_2 norm misfit between observed and predicted data out of the six different runs.

Notwithstanding the parallel implementation of the code and the limited number of unknowns (16 layers resulting in 48 unknowns that are the *Vp, Vs* and density of each inverted layer), the computer intensive elastic GA-FWI makes the application of this method to all the CDPs of the seismic line, prohibitive in terms of computational costs. For example, approximately 6 hours are required to complete the 16400 forward problems needed for a single CDP gather inversion. This results in approximately 1.5 days to complete the 6 inversion runs performed for each CDP gather. This computational time refers to the inversion performed on 2 compute nodes of a Linux cluster in which each compute node is a 2 esa-core Intel(R) Xeon(R) CPU E5645 at 2.4 GHz. For this reason we limited the stochastic inversion to only three CDP gathers selected along the seismic line as indicated in Figure 4. In the inversion the reflectivity method has been applied for forward modeling (Kennett, 1983). The band-pass filtered (5-10-37-50 Hz) version of the raw

CDP data constitutes the input for our 1D elastic GA-FWI because performing the inversion in a wider frequency range, although would greatly increases the resolution of the final result, would make the computational cost unaffordable. For this reason we have limited the inversion to frequencies below 50 Hz. Given the frequency band considered in the inversion, we set the layer thickness of the 1D model to 20 m. In fact, as shown by Mallick and Dutta (2002), the expected resolution of 1D full-waveform inversion is between 1/4 and 1/6 of the maximum wavelength associated with the dominant frequency. Being the well-site survey data single component (pressure only) and given the limited offset range (with a maximum offset of 600 m), the estimation of viscoelastic or anisotropy parameters is a hopelessly ill-conditioned problem as shown by Riedel and Theilen (2001) and Li and Mallick (2015). For what concerns the effects of attenuation, these play a minor role in controlling the reflection response if a narrow angular range of reflections is included in the inversion (Aleardi and Tognarelli, 2015). Therefore, we consider elastic and isotropic media.

Our 1D elastic FWI code is based on the stochastic optimization method known as niched genetic algorithm (Horn, 1993) in which the initial random population is divided in many subpopulations subjected to separated selection and evolution processes, with a possible exchange of some individuals only for a fixed number of iterations. This peculiar implementation is aimed at maximizing the exploration of the model space and at reducing the possibility for the algorithm to be stuck into local minima. Additional details about our code can be found in Aleardi and Mazzotti (2016). As it is widely known there is not a unique recipe to set the GA control parameters being their optimal setting very dependent on the type of problem to be solved and also on the personal preferences of the user. For this reason the optimal choice is usually found by a trial and error procedure. Here we only remind that one of the most important control parameters in a GA optimization is the total number of individuals that must be sufficiently high to ensure an efficient exploration of the entire model space and to prevent entrapment into local minima. Being the 1D elastic FWI a highly non-linear, multi-minima, optimization problem we set this number to 400 that is more than 8 times the number of unknowns. This entire population is divided into 5 subpopulations that evolve into 50 generations. We impose a selection rate of 0.8 that is the 80% of individuals in the current population is selected for recombination and mutation. Finally, we employ an elitist reinsertion, which preserves the fittest individuals of the previous generation in the new generation, combined with a fitness-based reinsertion in which the lowest-fitness parents are replaced by higher-fitness offspring.

4.1 FWI results: inversion using the entire waveform to compute the data misfit

In this first test, we consider the entire waveform in the computation of the L_2 norm misfit function between predicted and observed seismic data. The wavelet used as input for high-resolution velocity analysis is also used in the forward modelling to compute the predicted seismograms. A smoothed version of the velocity field previously derived from the high-resolution velocity analysis defines the *Vp* trend. To build the *Vs* trend we have assumed a *Vp/Vs* ratio that linearly varies from 6 at the seafloor interface to 2.2 at 400 m depth and scaled the *Vp* trend for this varying *Vp/Vs* ratio to obtain the *Vs* values. A linear function ranging from 1.3 to 2 when passing from the seabed to 400 m depth defines the density trend. The admissible parameter ranges in the inversion are +/-300 m/s for *Vp* and *Vs* and +/-0.3 g/cm^3 for density and are centred around their respective trends.

The estimation of the uncertainties associated to the inversion results is a good practice in solving geophysical optimization problems that usually are ill-conditioned and multi-minima (Tarantola, 2005). However, because GA's are not a Markov Chain Monte Carlo method, the direct use of the ensemble of GA-sampled models and their associated likelihoods produce biased uncertainty estimations (Sen and Stoffa, 1996), thus more sophisticated approaches are needed to derive reliable uncertainty quantifications after a GA optimization (see for example Sen and Stoffa, 1996; Aleardi, 2015b; Aleardi and Mazzotti, 2016; Sajeva *et al.* 2016b). This topic is beyond the extent of this work but as we are aware of the importance of at least a qualitative estimation of the ambiguities affecting the estimated models, we exploit the entire ensemble of GA-sampled models and their associated data misfit value to represent the final results. In particular, for each considered CDP gather we plot each sampled 1D model with a color scale that represent its data misfit value. The final results pertaining to CDP 100, CDP 250 and CDP 400 are illustrated in Figures 6, 7 and 8, respectively. In all cases we observe a linear and gradual increase for all of the parameters and significant *Vp* contrasts occur at 284 m and at 344 m below the sea level for CDP 100, at 284 m and at 364 m for CDP 250 and at 284 m and 384 m for CDP 400. In addition, Figures 6, 7 and 8 show that these *Vp* increases often correspond to *Vs* and density increases. However, the use of single component data and the limited offset range of the well-site survey acquisition make us more confident on the predicted *Vp* profiles than on the predicted *Vs* and density depth trends (Aleardi and Mazzotti, 2016). In fact, the greater ambiguity affecting *Vs* and density estimates is clearly illustrated by the colour maps in Figures 6, 7 and 8 where the morphology of the L_2 norm data misfit shows narrow valleys delimiting the predicted *Vp* profiles and larger and more flat valleys in the case of *Vs* and density predictions. This is a valuable information also in view of the fact that other additional and independent data (well log recordings or geotechnical data) are not available to further validate the results.

Although with different resolution capabilities, the *Vp* trends obtained by full-waveform inversion and by the high-resolution velocity analysis are in good agreement as shown in Figure 9. In particular, the two strong velocity contrasts below 280 m that are visible in the *Vp* profiles obtained by genetic algorithm FWI are also visible in the velocity field derived from the high-resolution velocity analysis. Figure 10 represents a comparison between observed, best predicted seismograms and their difference for the considered CDPs. A good match between observed and predicted data is attained in all cases. The differences between the observed and the predicted seismograms can be ascribed to residual noise contamination in the observed data and to physical assumptions that are made in the forward modelling computation (e.g., perfectly elastic propagation, homogeneous and isotropic 1D media), which may not be totally verified in this specific case. The average relative percentage errors resulting from the observed and the predicted data shown in Figure 10 are very similar for all the three considered CDPs and range between 26 and 28%.

4.2 FWI results: inversion using the trace envelope to compute the data misfit

We repeat the inversion for the CDP 400 considered in the previous example and using the same GA parameters, but in this test the envelopes (Sheriff *et al.* 1977) of the predicted and observed seismograms are used to compute the misfit between the observed and predicted seismic data. In practical applications an accurate source signature estimation is often problematic, especially for what concerns the estimation of the wavelet phase. For this reason, the envelope is sometimes used in solving the full-waveform inversion problem (Tognarelli et al. 2015, Galuzzi et al. 2016) as it permits to relax the assumption of a perfect estimation of the source signature phase.

Similarly to the previous examples we repeat this inversion 6 times from which we extract as the final estimated model the one resulting in the minimum misfit between observed and predicted data. Figure 11 shows the observed data envelope the predicted data envelope and their differences. Note that, disregarding the phase of the seismic wavelet, the final percentage error is 17.32%, a value lower than in all the previous cases that considered the entire waveforms (26-28%).

The final results are represented in Figure 12, where the best model obtained in the previous example and that obtained by considering the trace envelope are compared. The general depth trends are very similar, but some discrepancies are clearly visible below 300 m. In particular, the two *Vp* trends sometimes show a specular, symmetrical and opposite behaviour: some P-velocity increases predicted in the previous example show a reversal when considering the trace envelope. This may be because by using the envelope, the polarity of the reflection is lost and the same amplitude can then be referred to as either an increase or a decrease in acoustic impedance. Therefore, in elastic full-waveform inversion we may resort to using envelopes only in case the wavelet estimation is problematic or in a first run of the inversion to derive some additional information on the general velocity and density trends.

5. Conclusions

The properties of the shallowest part of the subsurface have been estimated from a 2D well-site survey data by applying two different methods: high-resolution velocity analysis, and 1D elastic full-waveform inversion solved with a genetic algorithm approach. The velocity analysis performed using the hybrid functional that exploits the high-frequency content of the considered data, is able to reduce the uncertainty in the velocity picking and derives a P-wave velocity field with a good degree of accuracy and with minimum computational effort. These velocity values can be used for preliminary interpretations or as a priori information for additional investigations, such as to define the search ranges of the model parameters in the GA-FWI.

To derive a complete elastic characterization of the shallowest part of the subsurface in the investigated area we use a 1D FWI solved with a genetic algorithm approach. Full-waveform inversion exploits all of the information contained in the recorded seismograms (different wave phenomena, amplitude and phase information) to derive a high-resolution subsurface model. FWI is a highly non-linear inverse problem characterized by a multi-minima misfit function. Differently from gradient-based inversion strategies, stochastic optimization methods, such as the genetic algorithms we employed, are able to explore different parts of the model space and to jump out from local minima, thus relaxing the need of a good starting model for all the inverted parameters. An additional advantage of genetic algorithms is that they can be easily parallelized thus reducing their high computational cost. To further reduce the computational cost we assume a 1D subsurface model, we limit the inversion to the shallowest part of the subsurface and, in particular, we exploit the outcomes derived from the high-resolution velocity analysis to reduce the search ranges for the unknown model parameters. In the FWI examples we discuss, we chose to consider a frequency band below 50 Hz, approximately, and this choice sets at 20 m the layers thickness for the inverted model. Fixing the maximum depth of the inverted models to 400 m, and considering that the first layer is the known water layer 84 m thick, a total of 16 layers and 48 unknowns results (the *Vp*, *Vs* and density of each inverted layer). Should we wish to reach a higher resolution, that is to decrease the layer thickness, a wider frequency range should be included in the inversion and this would results in an increase in the number of unknowns and in the computational cost. Therefore, in practical applications a compromise between the maximum resolution, the maximum depth of investigation, and the number of unknowns must be found, taking into consideration that the computational effort of the genetic algorithm full-waveform inversion grows exponentially with the number of unknowns and with the frequency ranges considered. Another limitation of the method is the assumption of a 1D subsurface model that restricts the applicability to very simple geological contexts or to seismic data gathers that have been properly migrated (Mallick, 1999). However, when the local 1D assumption is acceptable, such as in the data case we consider in this work, the 1D elastic FWI is a powerful method for deriving high-resolution subsurface models around a well-defined area of interest.

In this paper, the GA-FWI is performed by considering both the entire waveform and the envelope of the seismograms in computing the misfit between predicted and observed data. Some discrepancies, clearly related to the loss of polarity information caused by the envelope, are visible especially in the *Vp* profiles but the velocities and density depth trends are quite similar to those derived by using the entire waveform. To further prove the reliability of our results and to give a qualitative estimate of the uncertainties affecting the final predicted models, we use the entire information brought by the ensemble of GA-sampled models (in terms of misfit values and of sampled *Vp*, *Vs* and density values). From this analysis resulted that, as expected for single-component seismic data, *Vs* and density are the less resolvable parameters compared to the *Vp* one. Finally, despite the different resolutions, the stochastic FWI and the high-resolution velocity analysis yield comparable compressional velocity profiles with significant increases of velocity at shallow depth that may indicate the occurrence of a consolidated layer.

Concerning the general applicability of elastic full-waveform inversion, we think that stochastic FWI, due to its high computational cost, should be primarily thought as a target oriented approach useful to derive an accurate, but nevertheless very localized, elastic characterization of the subsurface. One possible further development is to consider the 1D elastic models predicted by GA-FWI to build a starting model for gradient-based full-waveform inversion (Tognarelli et al. 2016). In fact, differently from stochastic FWI, the gradient-based approach to full-waveform inversion, although limited by its local nature, is usually very fast to converge even in cases with many unknown model parameters (i.e. hundreds or thousands of unknowns). Therefore, gradient-based full-waveform inversion will enable us to relax the assumption of a local 1D geological model and to extend the frequency range considered in the genetic algorithm optimization, thus yielding final models with a significantly improved resolution.

Figures, Captions and Table

Table 1: Recording and acquisition parameters.

Recording and Acquisition Parameters	
Single Air Gun 150 cu. in.	Source and Streamer Depth 3 m
Shot Interval 12.5 m	Group Interval 12.5 m
Number of Shots 218	Minimum Offset 20 m
Streamer Length 600 m	Record Lenght 2048 ms
Number of Groups 48	Sample Rate 1 ms

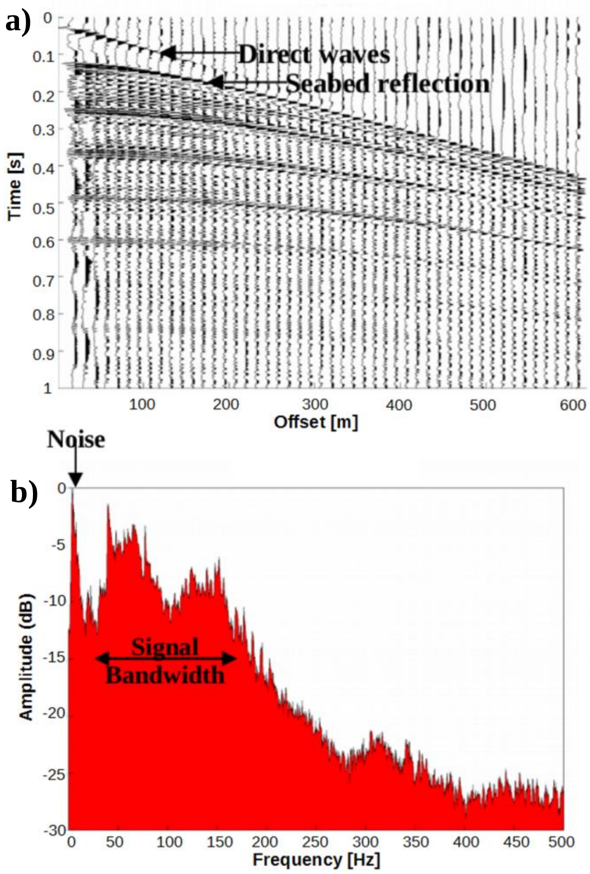

Figure 1: a) An example of raw shot gather. The direct waves and the seabed reflection are indicated. b) Average amplitude spectrum pertaining to the shot gather shown in a). The spectrum is characterized by low-frequency and high-amplitude noise at approximately 5 Hz, (see the black arrow). The signal bandwidth ranges between 10 Hz and 150 Hz, considering an amplitude level equal to -15 db. The typical slope related to the amplitude decay can be clearly observed from 150 Hz to 270 Hz.

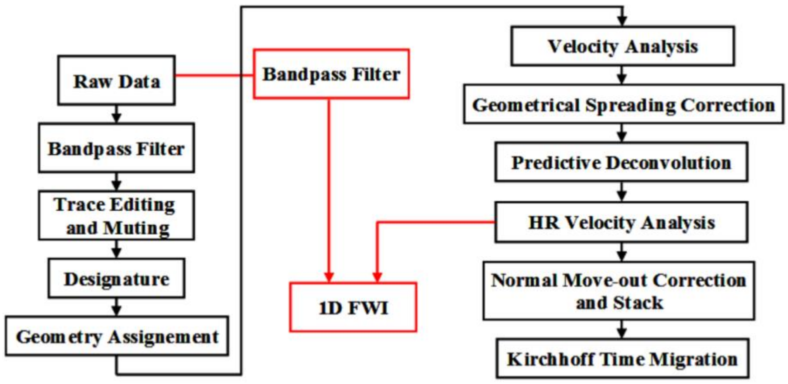

Figure 2: The processing sequence. The black arrows illustrate the flow used to obtain the final time-migrated section. The red arrows indicate the starting point of the input data for the 1D FWI.

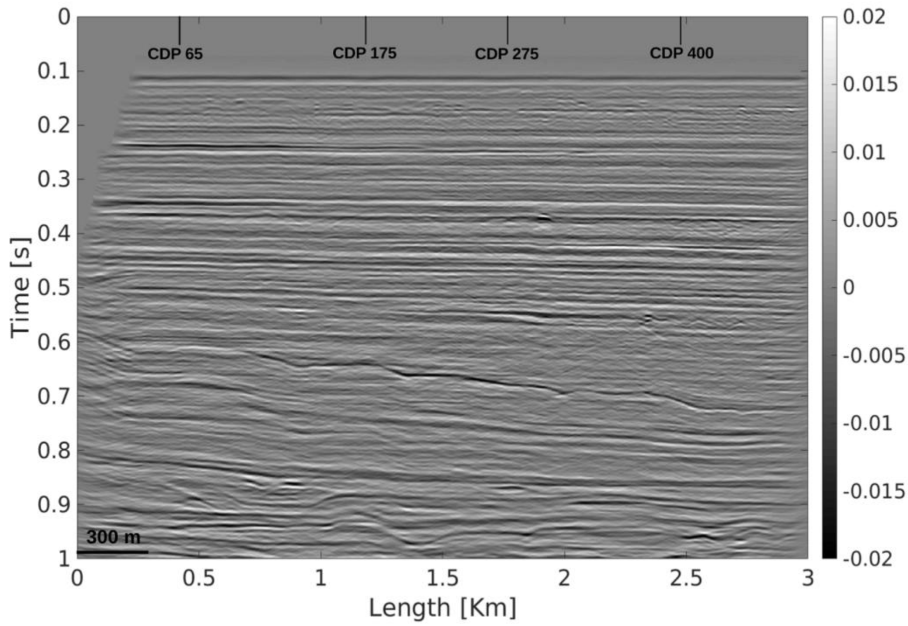

Figure 3: Time-migrated stack section at the end of the processing sequence shown in Figure 2. The locations of the four velocity spectra illustrated in Figure 4 (see section 3) are also shown. The high-resolution of the stack image can be appreciated particularly in the shallow part (down to 500 ms) that shows nearly horizontal reflectors. At higher two-way times, the layered structure becomes more complicated and the loss of high frequencies produces a significant decrease of resolution.

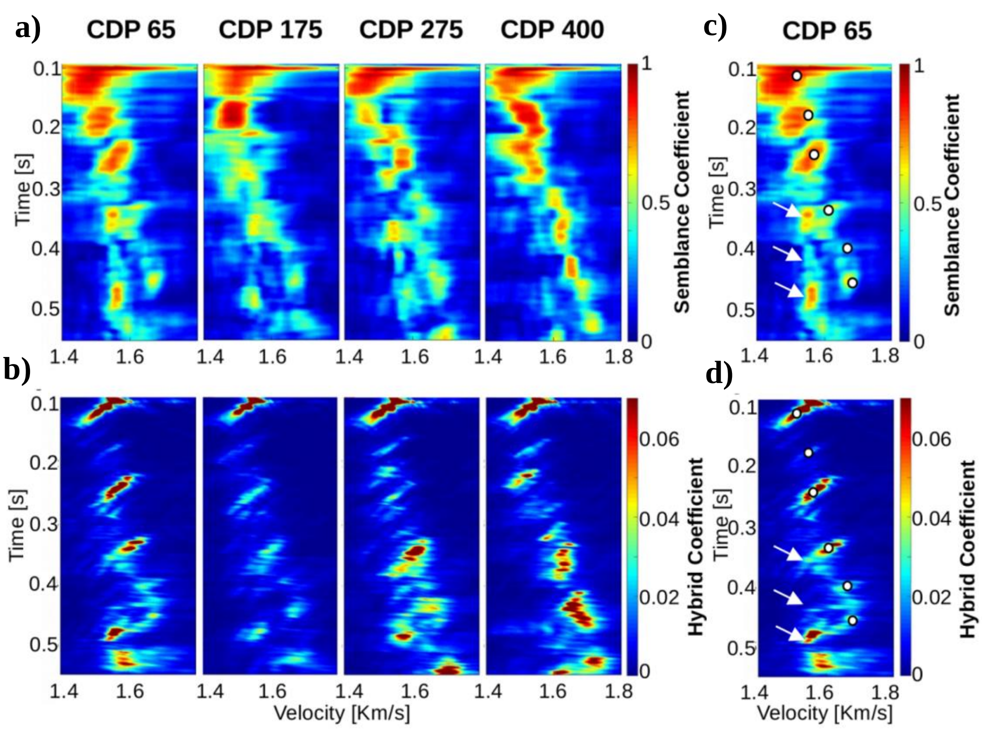

Figure 4: a) Velocity panels computed with the semblance functional C_{sem}.. b) Velocity panels computed with the C_{cmsKS} hybrid functional. The panels refer to CDP 65, 175, 275 and CDP 400. c) Velocity spectrum computed for CDP 65 making use of the semblance functional with superimposed the time-velocity pairs picked in the velocity panel shown in (d) computed with the hybrid functional C_{cmsKS} . In c) and d) the white arrows indicate the coherency maxima related to residual multiples. A different color scale is used to display the C_{sem} and C_{cmsKS} spectra due to the high dynamic range of the C_{cmsKS} functional. In a), b), c) and d) we represent the velocity panels from the arrival time of the seabed reflection (0.1 s, approximately) down to 0.52 s.

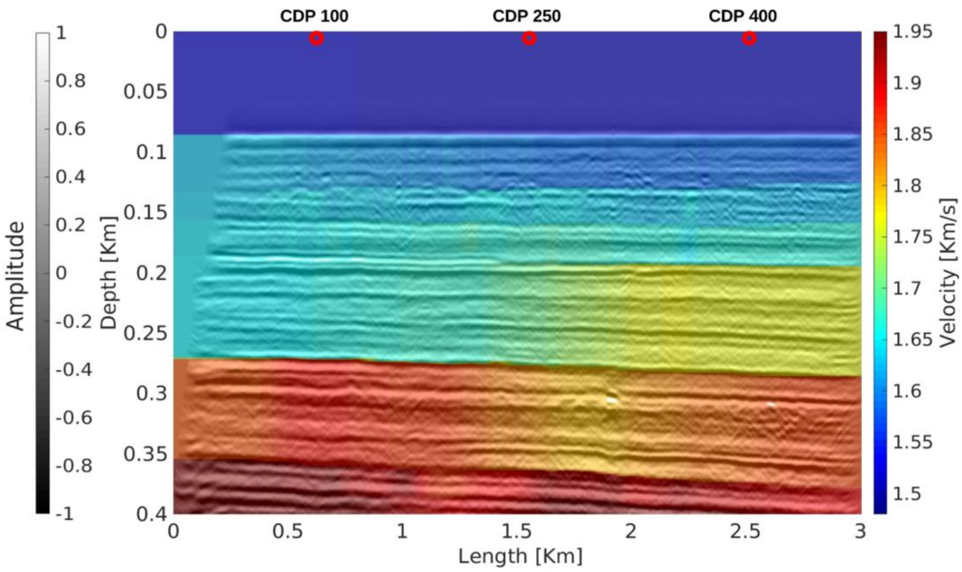

Figure 5: *Vp* model in depth obtained with the high-resolution velocity analysis. The depth migrated section is shown in background with grayscale. The positions of the CDP 100, CDP 250 and CDP 400, which will be considered in the FWI test, are also indicated.

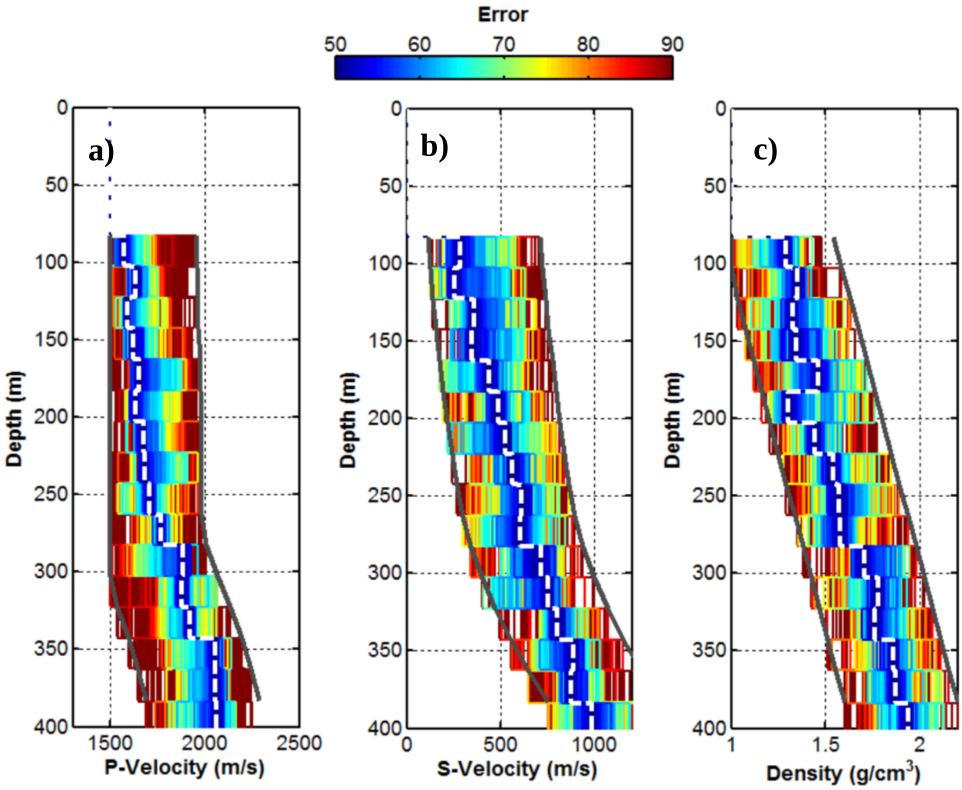

Figure 6: Results for the GA inversion for CDP 100. a), b) and c) show the estimated *Vp*, *Vs* and density depth trends (white dashed lines) and the parameter ranges considered in the GA inversion (gray continuous lines). The color lines depict the models explored during the GA inversion represented with their associated misfit value that is the L_2 norm between predicted and observed data. Note the narrow valley that delimits the predicted *Vp* profile and the larger and more flat valleys delimiting the *Vs* and density prediction. This is a qualitative evidence of the higher uncertainties associated with the *Vs* and density estimates with respect to those associated with the *Vp* ones. For a better comparison of the uncertainties the x-axes in a), b) and c) are represented with comparable ranges, that is a range of 1200 m/s for *Vp* and *Vs* and of 1.2 g/cm^3 for density.

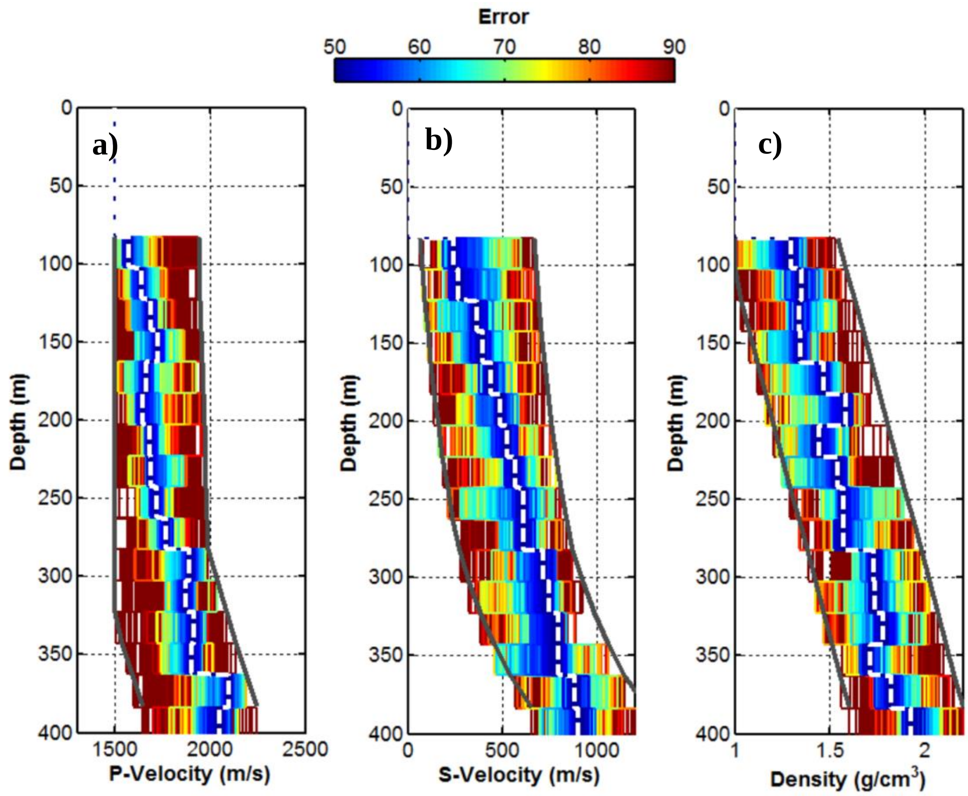

Figure 7: Same as in Figure 6 but for CDP 250.

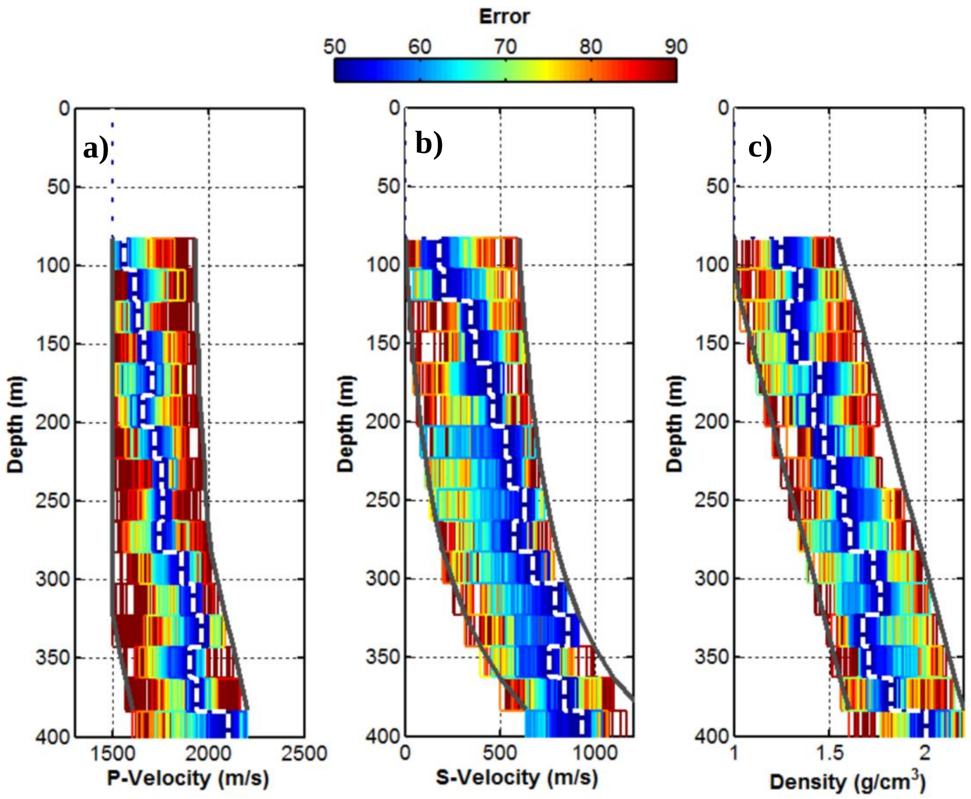

Figure 8: Same as in Figure 6 but for CDP 400.

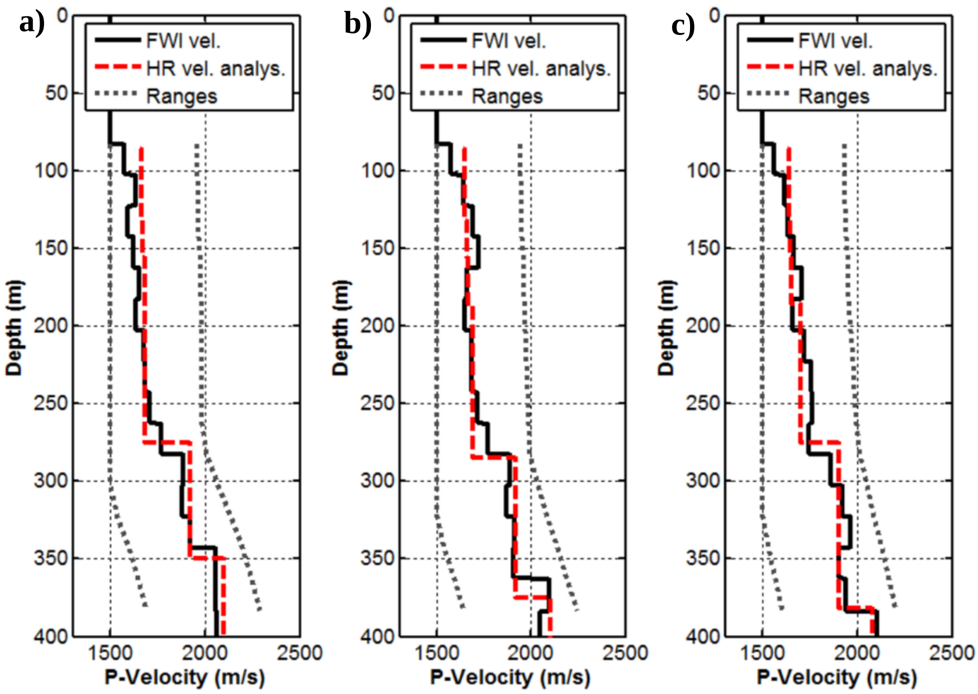

Figure 9: Comparison between the *Vp* profiles obtained by the high-resolution velocity analysis (red dashed lines) and by the 1D elastic GA-FWI (black continuous lines). a), b) And c) refer to the inversion of CDP 100, CDP 250 and CDP 400, respectively. The gray dotted lines represent the *Vp* ranges considered in the GA optimization. Note that, although with different resolution, the outcomes of high-resolution velocity analysis fair match the results produced by GA-FWI.

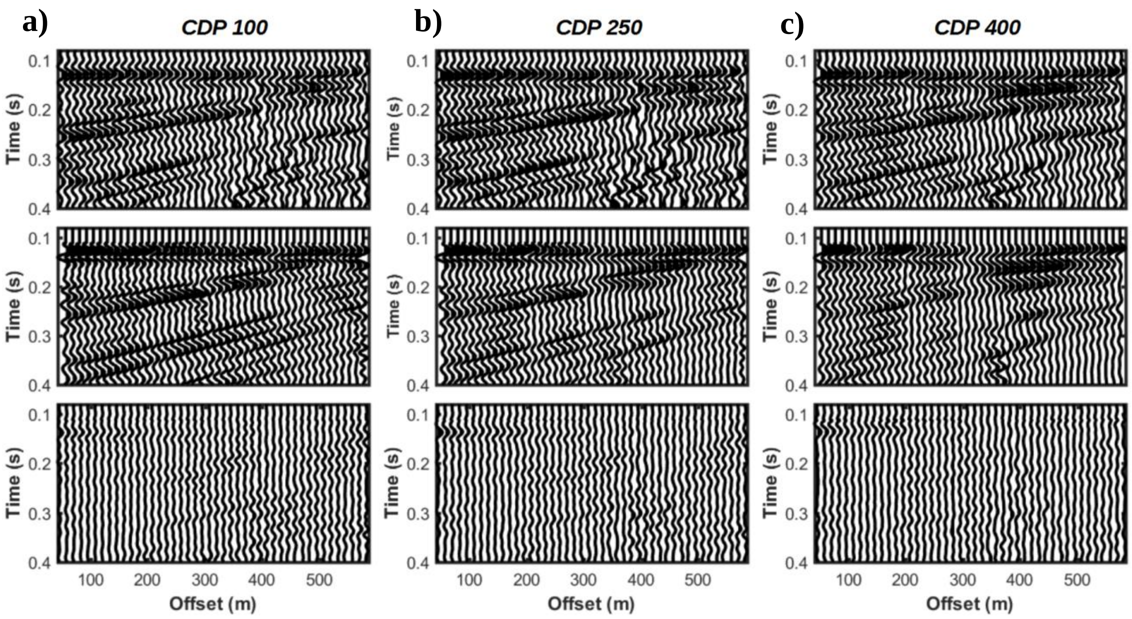

Figure 10: a), b) And c) represent a comparison between filtered observed data (top), predicted data (middle) and their difference (bottom) for CDP 100, CDP 250 and CDP 400, respectively. For a better comparison all the seismograms are represented with the same amplitude scale and are NMO corrected for the water velocity.

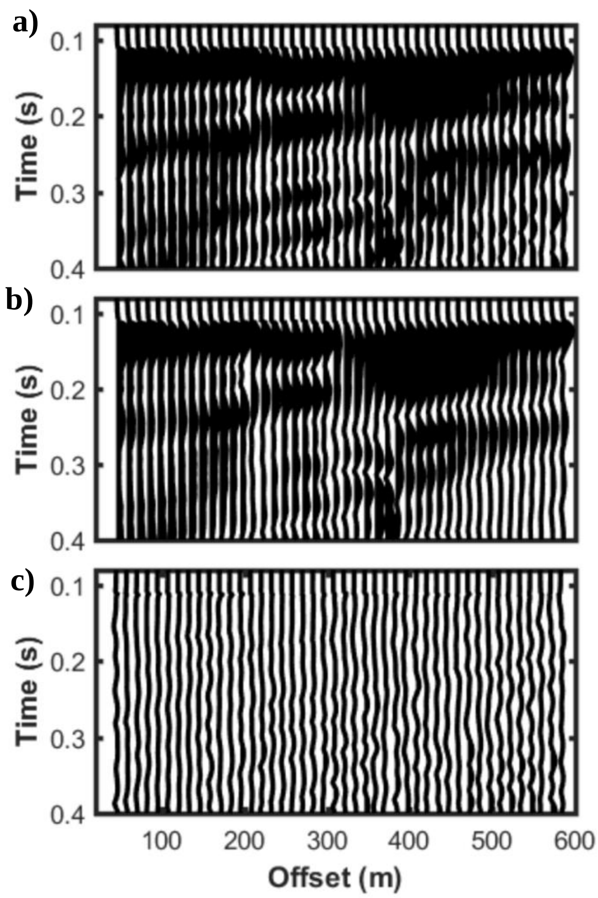

Figure 11: a), b) And c) comparison between the observed data envelope, the predicted data envelope and their differences, respectively. The resulting percentage error is 17.32 % that is lower than the percentage errors resulting from the inversion of the entire waveforms (see Figure 10).

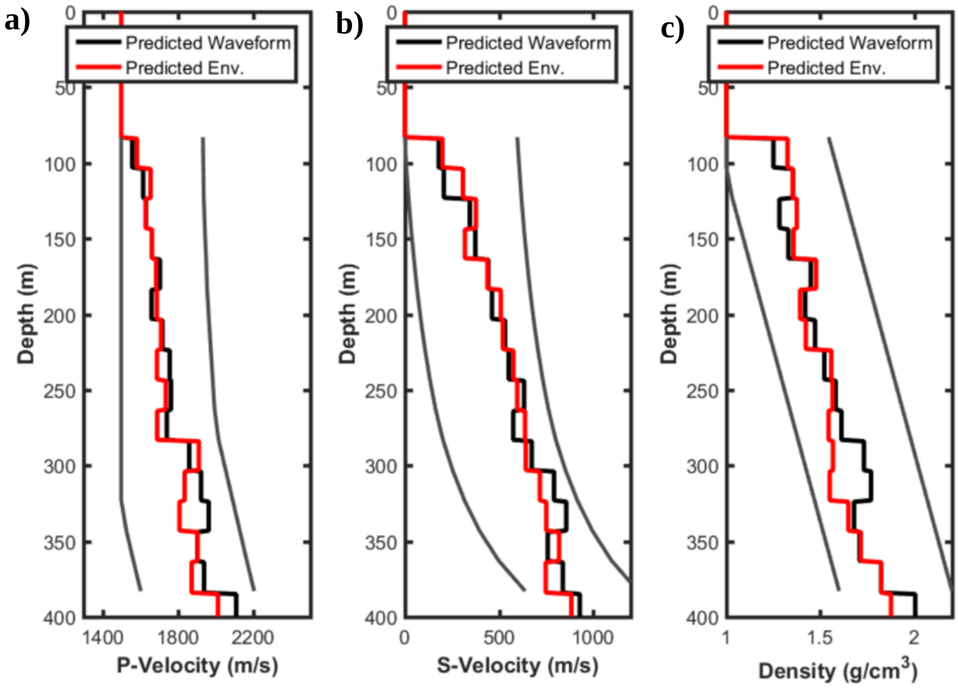

Figure 12: Comparison between the results obtained for CDP 400 by using the entire waveform (blue line) and the envelope (red line) in the misfit function. a), b) And c) illustrate the *Vp*, *Vs* and density depth trends, while the gray lines show the parameter ranges. Note that the predicted trends (especially for *Vp*) display some opposing and specular behaviour below 300 m.

References

Aleardi, M. 2015a. The importance of the Vp/Vs ratio in determining the error propagation, the stability and the resolution of linear AVA inversion: a theoretical demonstration. Bollettino di Geofisica Teorica e Applicata, 56(3), 357-366.

Aleardi, M. 2015b. Seismic velocity estimation from well log data with genetic algorithms in comparison to neural networks and multilinear approaches. Journal of Applied Geophysics, 117, 13-22.

Aleardi, M., and Mazzotti, A. 2014. 1D Elastic FWI and Uncertainty Estimation by Means of a Hybrid Genetic Algorithm-Gibbs Sampler Approach. In 76th EAGE Conference and Exhibition 2014. doi: 10.3997/2214-4609.20140858

Aleardi, M., and Mazzotti, A. 2016. 1D elastic full-waveform inversion and uncertainty estimation by means of a genetic algorithm-Gibbs sampler approach. Geophysical Prospecting. doi: 10.1111/1365-2478.12397.

Aleardi, M., and Tognarelli, A. 2015. The Limits of Narrow and Wide Angle AVA Inversions in Case of High Vp/Vs Ratios-Application to Seabed Characterization. In Near Surface Geoscience 2015-21st European Meeting of Environmental and Engineering Geophysics. doi: 10.3997/2214-4609.201413803

Aleardi, M., and Tognarelli, A. 2016. The limits of narrow and wide-angle AVA inversions for high Vp/Vs ratios: An application to elastic seabed characterization. Journal of Applied Geophysics, 131, 54-68.

Abbad, B., and Ursin, B. 2012. High-resolution bootstrapped differential semblance: Geophysics, 77(3), U39–U47. doi: 10.1190/geo2011-0231.1

Abbad, B., Ursin, B. and Rappin, D. 2009. Automatic nonhyperbolic velocity analysis: Geophysics, 74(2), U1–U12. doi: 10.1190/1.3075144

Ashton, C. P., Bacon, B., Mann, A., Moldoveanu, N., Déplanté, C., Ireson, D., Sinclair, T. and Redekop, G. 1994. 3D seismic survey design. Oilfield Review, 6(2), 19-32.

Biondi, B. L., and Kostov, C. 1989. High-resolution velocity spectra using eigenstructure methods: Geophysics, 54, 832–842. doi: 10.1190/1.1442712

Diouane, Y., Calandra, H., Gratton, S., and Vasseur, X. 2014. A Parallel Evolution Strategy for Acoustic Full-Waveform Inversion. In EAGE Workshop on High Performance Computing for Upstream. doi: 10.3997/2214-4609.20141923

Fliedner, M.M., Treitel, S., and MacGregor, L. 2012. Full-waveform inversion of seismic data with the Neighborhood Algorithm. The Leading Edge, 31(5), 570-579.

Galuzzi, B., Tognarelli, A., Stucchi, E., and Mazzotti, A. 2016. Stochastic FWI on Wide-angle Land Data with Different Order of Approximation of the 2D Acoustic Wave Equation. In 78th EAGE Conference and Exhibition 2016. doi: 10.3997/2214-4609.201601189.

Goldberg, D.E. 1989. Genetic algorithms in search, optimization, and machine learning. Reading Menlo Park: Addison-wesley.

Grandi, A., Mazzotti, A., and Stucchi, E. 2007. Multicomponent velocity analysis with quaternions. Geophysical Prospecting, 55, 761–777.

Holland, J.H. 1975. Adaptation in natural and artificial systems: An introductory analysis with applications to biology, control, and artificial intelligence. University Michigan Press.

Horn, J. 1993. Finite Markov chain analysis of genetic algorithms with niching. Forrest, 727, 110-117.

Jones, I. F., and Levy, S. 1987. Signal-to-noise ratio enhancement in multichannel seismic data via the Karhunen-Loève transform: Geophysical Prospecting, 35, 12–32. doi: 10.1111/j.1365-2478.1987.tb00800.x.

Jones, I.F., 2010. An introduction to velocity model building. EAGE, ISBN 978-90-73781-84-9, 296 pages.

Kennett, B. L. 1983. Seismic wave propagation in stratified media. Cambridge University Press.

Key, S.C., and Smithson, S.B. 1990. New approach to seismic-reflection event detection and velocity determination. Geophysics, 55(8), 1057-1069.

Larner, P., and Celis, V. 2007. Selective-correlation velocity analysis. Geophysics, 72, 11-19.

Li, T., and Mallick, S. 2015. Multicomponent, multi-azimuth pre-stack seismic waveform inversion for azimuthally anisotropic media using a parallel and computationally efficient non-dominated sorting genetic algorithm. Geophysical Journal International, 200(2), 1134-1152.

Mallick, S. 1999. Some practical aspects of prestack waveform inversion using a genetic algorithm: An example from the east Texas Woodbine gas sand. Geophysics, 64(2), 326-336.

Mallick, S., and Dutta, N.C. 2002. Shallow water flow prediction using prestack waveform inversion of conventional 3D seismic data and rock modeling. The Leading Edge, 21(7), 675-680.

Mazzotti, A., and Ravagnan, G. 1995. Impact of processing on the amplitude versus offset response of a marine seismic data set. Geophysical Prospecting, 43(3), 263-281.

Mitchell, M. 1998. An introduction to genetic algorithms. MIT press.

Morgan, J., Warner, M., Bell, R., Ashley, J., Barnes, D., Little, R., Roele, K. and Jones, C. 2013. Next-generation seismic experiments: wide-angle, multi-azimuth, three-dimensional, full-waveform inversion. Geophysical Journal International, 195(3), 1657-1678.

Neidell, N. S., and Taner, M. T. 1971. Semblance and other coherency measures for multichannel data. Geophysics, 36, 482-497.

Operto, S., Gholami, Y., Prieux, V., Ribodetti, A., Brossier, R., Metivier, L., & Virieux, J. 2013. A guided tour of multiparameter full-waveform inversion with multicomponent data: From theory to practice. The Leading Edge, 32(9), 1040-1054.

Prieux, V., Brossier, R., Gholami, Y., Operto, S., Virieux, J., Barkved, O. and Kommedal, J. 2011. On the footprint of anisotropy on isotropic full waveform inversion: The Valhall Case Study. Geophysical Journal International, 187, 1495–1515.

Riedel, M., and Theilen, F. 2001. AVO investigations of shallow marine sediments. Geophysical Prospecting, 49(2), 198-212.

Riedel, M., Dosso, S. E., and Beran, L. 2003. Uncertainty estimation for amplitude variation with offset (AVO) inversion. Geophysics, 68(5), 1485-1496.

Sacchi, M. D. 1998. A bootstrap procedure for high-resolution velocity analysis. Geophysics, 63, 1716-1725. doi: 10.1190/1.1444467

Sajeva, A., Aleardi, M., Mazzotti, A., Bienati, N., and Stucchi E. 2014a. Estimation of velocity macro-models using stochastic full-waveform inversion. SEG Technical Program Expanded Abstracts, 1227-1231. doi: 10.1190/segam2014-1088.1

Sajeva, A., Aleardi, M., Mazzotti, A., Stucchi, E., and Galuzzi, B. 2014b. Comparison of Stochastic Optimization Methods on Two Analytic Objective Functions and on a 1D Elastic FWI. In 76th EAGE Conference and Exhibition 2014. doi: 10.3997/2214-4609.20140857.

Sajeva, A., Aleardi, M., Stucchi, E., Bienati, N., Mazzotti, A., 2016a. Estimation of acoustic macro-models using genetic full-waveform inversion: applications to the Marmousi model. Geophysics, 81(4), R173-R184.

Sajeva A., Aleardi M., Mazzotti A., 2016b. Combining genetic algorithms, Gibbs sampler, and gradient-based inversion to estimate uncertainty in 2D FWI. In 78th EAGE Conference and Exhibition 2016. DOI: 10.3997/2214-4609.201601543.

Sen, M. K., and Stoffa, P. L. 1996. Bayesian inference, Gibbs' sampler and uncertainty estimation in geophysical inversion. Geophysical Prospecting, 44(2), 313-350.

Sguazzero, P., and Vesnaver, A. 1987. A comparative analysis of algorithms for seismic velocity estimation. In Bernabini M., Rocca F., Treitel S. and Worthington M., Eds., Deconvolution and inversion. Blackwell Scientific Publications, 267-286.

Sheriff, R.E., Taner, M.T., Koehler, F., and Frye, D. 1977. Extraction and interpretation of the complex seismic trace. In Proceedings of the 6th convention of the Indonesian Petroleum Association, 305-316.

Sivanandam, S. N., and Deepa, S. N. 2008. Genetic Algorithm Optimization Problems. Springer Berlin Heidelberg.

Sirgue, L., Barkved, O.I., Dellinger, J., Etgen, J., Albertin, U. and Kommedal, J.H. 2010. Full waveform inversion: The next leap forward in imaging at Valhall. First Break, 28, 65–70.

Spagnolini, U., Caciotta, L., and Manni, A. 1993. Velocity analysis by truncated singular value decomposition. SEG Technical Program Expanded Abstracts, 677-680. doi: 10.1190/1.1822586

Tarantola, A. 2005. Inverse problem theory and methods for model parameter estimation. Siam.

Tognarelli, A., Stucchi, E., Ravasio, A., and Mazzotti, A. 2013. High-resolution coherency functionals for velocity analysis: An application for subbasalt seismic exploration. Geophysics, 78(5), U53-U63.

Tognarelli A., Stucchi, E.M., Bienati, N., Sajeva, A., Aleardi, M., and Mazzotti, A. 2015. Two grid stochastic Full Waveform Inversion of 2D Marine Seismic Data. In 77th EAGE Conference and Exhibition 2015. doi: 10.3997/2214-4609.201413197

Tognarelli, A., Aleardi, M., Mazzotti, M., 2016. Estimation of a high resolution P-wave velocity model of the seabed layers by means of global and a gradient-based FWI. Submitted for Near Surface Geoscience 2016-22nd European Meeting of Environmental and Engineering Geophysics.

Virieux, J., and Operto, S. 2009. An overview of full-waveform inversion in exploration geophysics. Geophysics, 74(6), WCC1-WCC26.